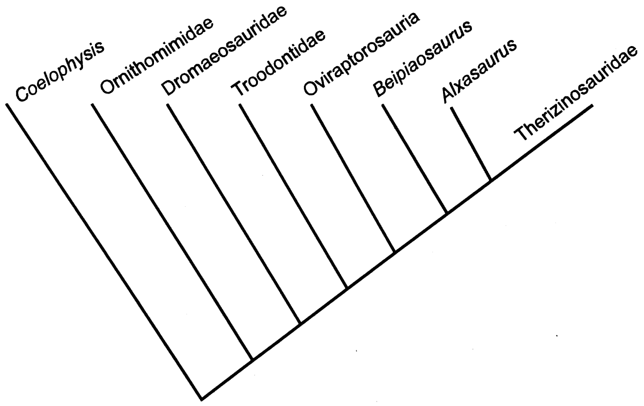

Figure 4 Phylogenetic relationships of *Beipiaosaurus inexpectus*. *Beipiaosaurus* and other therizinosauroids share 18 synapomorphies, including the following unique characters: a prominent dorsolateral shelf on the dentary (21.1), teeth that increase in size anteriorly (25.1), tooth crowns with sub-circular basal cross-sections that lack mediolateral compression (27.1), anteroposteriorly narrow and dorsoventrally deep pubic peduncle of ilium (46.1 and 47.1), very deep proximal end of manual unguals (70.1), short metatarsus (78.1) and reduced main body of astragalus (82.1). It is less derived than other therizinosauroids because it lacks 13 characters of Therizinosauroidea (1.1, 36.1, 38.0, 43.0, 48.1, 49.1, 51.1, 52.1, 58.1, 60.0, 66.0, 77.1, 79.1), including the following unusual characters: a very small head (1.1), the long and deep preacacetabular portion of ilium (48.1 nd 49.1) and absence of the theropod first metatarsal (79.1).

theropods[8–11]. Given this phylogeny (Fig. 4), some derived characters of therizinosauroids other than *Beipiaosaurus* are most parsimoniously interpreted as having evolved convergently with some other dinosaur groups, sauropodomorphs in particular. Thus, therizinosauroids re-evolved a robust first digit in which the proximal end of metatarsal I articulates with the tarsals (79.1).

Feathers are complex structures. Their abrupt appearance in the bird fossil record has been difficult to explain, mainly because no intermediate structures are preserved in the related theropod taxa. The integumentary filaments of *Sinosauropteryx* have been considered to be ‘proto-feathers’ by some, but this idea has been rejected by others[26]. Such structures have not been preserved with any other theropods[26] until the discovery of *Beipiaosaurus*. The filamentous structures in *Beipiaosaurus* are similar to, but longer than, those of the compsognathid *Sinosauropteryx*. They are perpendicular to the limb bones, and are unlikely to be muscle fibres or frayed collagen[27]. Their presence in both therizinosauroids and compsognathids indicates that there may be a broader distribution of similar structures in theropod dinosaurs. This supports the idea that these simple integumentary filaments may represent an intermediate evolutionary stage to the more complex feathers of *Protarchaeopteryx*, *Caudipteryx*[16] and more derived Avialae. The absence of such structures in most theropod fossils is probably attributable to the lack of such ideal preservation as is found in the Yixian Formation. This again indicates that feathers preceded flight[16], because both therizinosaurids and compsognathids apparently could not fly and did not descend from flying animals. □

Received 4 November 1998; accepted 31 March 1999.

1. Paul, G. S. The segnosaurian dinosaurs: relics of the prosauropod-ornithischian transition. *J. Vert. Paleontol.* **4,** 507–515 (1984).
2. Gauthier, J. A. Saurischian monophyly and the origin of birds. *Mem. Calif. Acad. Sci.* **8,** 1–55 (1986).
3. Sereno, P. C. Prosauropod monophyly and basal sauropodomorph phylogeny. *J. Vert. paleontol.* (suppl.) **9,** 38A (1989).
4. Perle, A. Segnosauridae—a new family of theropods from the Late Cretaceous of Mongolia. *Trans. Joint Soviet–Mongolian Palaeontological Expedition* **8,** 45–55 (1979).
5. Perle, A. A new segnosaurid from the Upper Cretaceous of Mongolia. *Trans. Joint Soviet–Mongolian Palaeontological Expedition* **15,** 28–39 (1981).
6. Barsbold, R. & Perle, A. Segnosauria, a new infraorder of carnivorous dinosaurs. *Acta Palaeontol. Pol.* **25**(2), 187–195 (1980).
7. Barsbold, R. Carnivorous dinosaurs from the Cretaceous of Mongolia. *Trans. Joint Soviet–Mongolian Palaeontological Expedition* **19,** 1–116 (1983).
8. Russell, D. A. & Dong, Z. The affinities of a new theropod from the Alxa Desert, Inner Mongolia, China. *Can. J. Earth Sci.* **30,** 2107–2127 (1993).
9. Clark, J. M., Perle, A. & Norell, M. A. The skull of *Erlicosaurus andrewsi*, a Late Cretaceous “Segnosaur” (Theropod: Therizinosauridae) from Mongolia. *Am. Mus. Novit.* **3115,** 1–39 (1994).
10. Sues, H.-D. On *Chirostenotes*, a Late Cretaceous Oviraptorosaur (Dinosauria: Theropod) from Western North America. *J. Vert. Paleontol.* **17,** 498–716 (1997).
11. Makovicky, P. & Sues, H.-D. Anatomy and phylogenetic relationships of the theropod dinosaur *Microvenator celer* from the Lower Cretaceous of Montana. *Am. Mus. Novit.* **3240,** 1–27 (1998).
12. Barsbold, R. & Maryanska, T. in *The Dinosauria* (eds Weishampel, D. B., Dodson, P. & Osmolska, H.) 408–415 (Univ. California Press, Berkeley, 1990).
13. Swisher, C. C., Wang, Y.-q., Wang, X.-l, Xu, X. & Wang, Y. $^{40}Ar/^{39}Ar$ dating of the lower Yixian Fm., Liaoning Province, northeastern China. *Chinese Sci. Bull.* (suppl.) **43,** 125 (1998).
14. Ji, Q. & Ji, S. A. On discovery of the earliest bird fossil in China and the origin of birds. *Chinese Geol.* **233,** 30–33 (1996).
15. Chen, P.-j., Dong, Z.-m. & Zhen, S.-A. An exceptionally well preserved theropod dinosaur from the Yixian Formation of China. *Nature* **391,** 147–152 (1998).
16. Ji, Q., Currie, P. J., Norell, M. A. & Ji, S.-A. Two feathered dinosaurs from northeastern China. *Nature* **393,** 753–761 (1998).
17. Martin, L. D. in *Origins of Higher Groups of Tetrapods* (eds Schultz, H.-P. & Treube, L.) 485–540 (Cornell Univ. Press, Ithaca, N. Y., 1991).
18. Bellairs, A. D’A. & Jenkin, C. R. in *Biology and Comparative Physiology of Birds* Vol. 9 (ed. Marshall, A.) 241–300 (Academic, New York, 1960).
19. Perle, A., Chiappe, L. M., Barsbold, R., Clark, J. M. & Norell, M. A. Skeletal morphology of *Mononykus olecranus* (Theropod, Avialae) from the Late Cretaceous of Mongolia. *Am. Mus. Novit* **3105,** 1–29 (1994).
20. Ostrom, J. H. Osteology of *Deinonychus antirrhopus*, an unusual theropod from the Lower Cretaceous of Montana. *Bull. Peabody Mus. Nat. Hist., Yale Univ.* **30,** 1–165 (1969).
21. Ji, Q. & Ji, S. A. Protarchaeopterygid bird (*Protarchaeopteryx* gen. nov.)-fossil remains of archaeopterygids from China. *Chinese Geol.* **238,** 38–41 (1997).
22. Russell, D. A. in *Encyclopedia of Dinosaurs* (eds Currie, P. J. & Padian, K.) 729–730 (Academic, San Diego, 1997).
23. Norell, M. & Makovicky, P. J. Important features of the *Dromaeosaur* skeleton: information from a new specimen. *Am. Mus. Novit.* **3215,** 1–28 (1997).
24. Chiappe, L., Norell, M. A. & Clark, J. Phylogenetic position of *Mononykus* (Aves: Alvarezauridae) from the Late Cretaceous of the Gobi Desert. *Mem. Queensland Mus.* **39,** 557–582 (1996).
25. Zhao, X. & Xu, X. The oldest coelurosaurian. *Nature* **394,** 234–235 (1998).
26. Unwin, D. M. Feathers, filaments and theropod dinosaurs. *Nature* **391,** 119–120 (1998).
27. Gibbons, A. Plucking the feathered dinosaur. *Science* **278,** 1229 (1997).

Supplementary information is available on *Nature*’s World-Wide Web site (http://www.nature.com) or as paper copy from the London editorial office of *Nature*.

Acknowledgements. We thank J. Clark for advice and reviewing the manuscript; Z.-X. Luo for improving the organization and language of the manuscript as well as the use of PAUP 3.11; Z.-H. Zhou and O. Rauhut for discussions; P. Currie, M. Norell, P. Sereno, X.-C. Wu and H. Osmolska for reviews and comments; and the Liaoxi expedition members of the IVPP. Photographs were taken by J. Zhang, electronic photography by L. Oyang, and line drawings are by R.-S. Li, Y.-T. Li, H.-J. Wang and J.-Z. Ding prepared the specimen. This study was supported by research grants from the Chinese Academy of Sciences and the National Natural Science Foundation of China.

Correspondence and requests for materials should be addressed to X.X. (e-mail: xxu@sun.midwest.com.cn).

Complex dynamics and phase synchronization in spatially extended ecological systems

Bernd Blasius, Amit Huppert & Lewi Stone

The Porter Super-Center for Ecological and Environmental Studies & Department of Zoology, Tel Aviv University, Ramat Aviv, Tel Aviv 69978, Israel

Population cycles that persist in time and are synchronized over space pervade ecological systems, but their underlying causes remain a long-standing enigma[1–11]. Here we examine the synchronization of complex population oscillations in networks of model communities and in natural systems, where phenomena such as unusual ‘4- and 10-year cycle’ of wildlife are often found. In the proposed spatial model, each local patch sustains a three-level trophic system composed of interacting predators, consumers and vegetation. Populations oscillate regularly and periodically in phase, but with irregular and chaotic peaks together in abundance—twin realistic features that are not found in standard ecological models. In a spatial lattice of patches, only small amounts of local migration are required to induce broad-scale ‘phase synchronization’[12,13], with all populations in the lattice phase-locking to the same collective rhythm. Peak population abundances, however, remain chaotic and largely uncorrelated. Although synchronization is often perceived as being detrimental

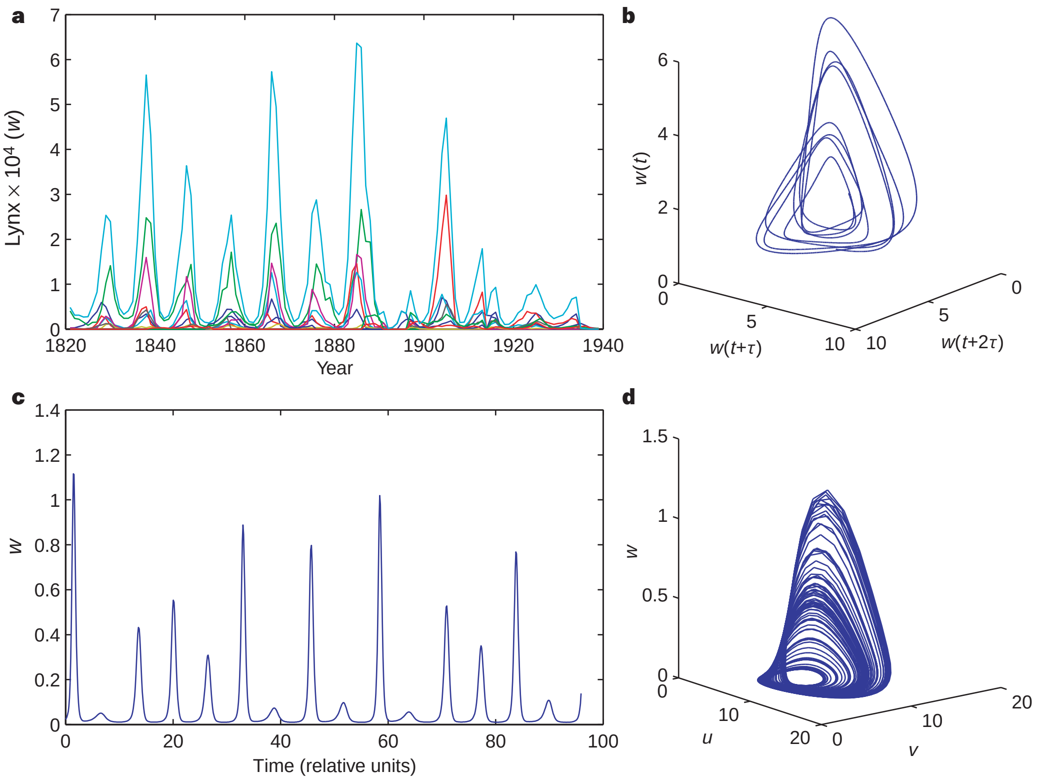

Figure 1 Time series analysis. **a**, Time series of lynx abundances (1821–1934) from six regions in Canada. Data are from ref. 1. **b**, Reconstructed attractor of hare–lynx system obtained by spatially averaging all regional lynx data and embedding the resulting time-series $w(t)$ using lagged coordinates, $w(t)$ versus $w(t+3)$ versus $w(t+6)$ after filtering and interpolating[11]. The dynamics of the full three-dimensional system is reconstructed from the time series of the single lynx variable. The attractor 'folds' in three-dimensional space, showing the chaotic cycling between predator, prey and vegetation. **c**, Time series of model (equation (1)) predator population w with chaotic dynamics. **d**, The model's hare–lynx–vegetation attractor, obtained by plotting u versus v versus w, has a similar structure to that found in **a**.

to spatially structured populations[14], phase synchronization leads to the emergence of complex chaotic travelling-wave structures which may be crucial for species persistence.

Ecological systems and their component biological populations exhibit a broad range of non-equilibrium dynamics, from characteristic natural cycles to more complex chaotic oscillations[15–17]. Here we examine a common but intriguing class of ecological cycle in which the frequency of a population remains relatively constant over time but in which there are erratic changes in abundance. A striking example of this is the well known hare–lynx cycle[1–11]. Despite unpredictable population fluctuations from one cycle to the next in the snowshoe hare (*Lepus americanus*) and the Canadian lynx (*Lynx canadensis*), the overall oscillation tends to follow a tight rhythm with a period of ~10 years[11] (Fig. 1a). Hare and lynx

Box 1 The chaotic UPCA foodweb model

We used the following vertical foodweb model with vegetation (u), herbivores (v) and predators (w):

$$\begin{aligned}\dot{u} &= au \qquad - \alpha_1 f_1(u,v)\\ \dot{v} &= -bv \quad + \alpha_1 f_1(u,v) - \alpha_2 f_2(v,w)\\ \dot{w} &= -c(w-w^*) \qquad + \alpha_2 f_2(v,w)\end{aligned} \tag{1}$$

Parameters a, b and c represent the respective growth rates of each trophic species in the absence of interspecific interactions. Predator–prey and consumer–resource interactions are incorporated into the equations using either the Lotka–Volterra term, $f_i(x,y) = xy$, or the Holling type II term, $f_i(x,y) = xy/(1+k_i x)$, with strengths set by the coefficients α_i. We also generalize the model by allowing the predator w to maintain a low equilibrium level $w = w^*$ even when its usual prey, v, is rare. This might arise when there are alternative food sources available for the predator[22], and is modelled by linearizing the predators' growth rate in equation (1) about the equilibrium by using the term $(w - w^*)$. These equations might, for example, outline the principal ecological transfers involved in the Canadian lynx–hare–vegetation foodweb, whose dynamics are dependent on three vertical trophic levels[3,28] and where alternative prey (such as the red squirrel) are considered to be important for the lynx population[29].

For the simulation runs reported here, we used the following parameters: $a = 1$, $b = 1$, $c = 10$, $\alpha_1 = 0.2$, $\alpha_2 = 1$, $k_1 = 0.05$, $k_2 = 0$, $w^* = 0.006$. f_1 and f_2 were taken as Holling type II and Lotka–Volterra interaction terms, respectively, although different combinations have been used successfully in other model variants. Chaotic dynamics were diagnosed from a study of the model's lyapunov exponent, calculated as in ref. 30.

In an N-patch system, migration to the ith patch is modelled as follows:

$$\begin{aligned}\dot{u}_i &= au_i \qquad - \alpha_1 f_1(u_i,v_i)\\ \dot{v}_i &= -b_i v_i \quad + \alpha_1 f_1(u_i,v_i) - \alpha_2 f_2(v_i,w_i) + D\Sigma_j(v_j - v_i)\\ \dot{w}_i &= -c(w_i - w^*) \qquad + \alpha_2 f_2(v_i,w_i) + D\Sigma_j(w_j - w_i)\end{aligned} \tag{2}$$

w_i represents the predator population in the ith patch and D sets the magnitude of diffusive migration summed over a predefined set of local nearest neighbours $\{j\}$. Lattice simulations (as in Fig. 5), were obtained for free and periodic boundaries in $N \times N$ lattices for N values of 20, 50 and 100, and with coupling through 4 and 8 nearest neighbours. Results were robust to these changes in model configuration.

populations from different regions of Canada synchronize in phase to a collective cycle that manifests over millions of square kilometres[1–10]. Similar spatially synchronized fluctuations are seen in many biological, ecological and epidemiological contexts and may involve disparate animal taxa across widely separated sites[7–10,18].

There are many possible explanations for spatially synchronized population oscillations. It has been suggested that extrinsic large-scale climatic forcing may often be responsible for entraining populations over vast geographic distances[7]. Intrinsic predator–prey and consumer–resource relationships within the foodweb, including density-dependent and time-delayed effects, may also generate population cycling, with local migration enhancing spatial synchronization[6,9,10]. The large number of ecological processes involved underscores the need to develop a deterministic 'strategic model'[2] that can realistically reproduce these complex population dynamics. A simply formulated robust tritrophic foodweb model achieves this goal and provides the necessary framework for studying ecological synchronization effects. The minimal model consists of a three-level 'vertical' food chain with predators (w) feeding on herbivores (v), which consume vegetation (u), and is described in Box 1.

This novel skeleton model generates surprisingly complex dynamics, including equilibrium and limit-cycle behaviour, and large parameter ranges for which there is an interesting class of chaotic oscillation. Figure 1c shows a time series of the predator population (w) for a typical model run in the chaotic regime. The predator, like all model populations, oscillates with a frequency Ω that is practically constant[12], as the community trajectory rotates at a uniform phase rate around the 'attractor' (Fig. 1d). Despite this regular rhythm in phase, the peak population abundance in each cycle appears to be highly unpredictable. These twin features of uniform phase evolution and chaotic amplitude (UPCA) are similar to those of the Canadian hare–lynx system[11], as is evident from comparing their respective time series and underlying 'attractors' (Fig. 1). The model lynx population achieves a cycle-amplitude variability (ratio of maximum to minimum population density) of 12–150, which is very close to recorded field values[9]. Although other deterministic tritrophic models also yield chaotic oscillations[4,19–21], none reproduces both the regular recurring rhythm and the smooth but irregular rises and falls in population abundances (the UPCA) fundamental to equation (1) and the observed hare-lynx data.

The population model (Box 1, equation (1)) represents a single isolated 'patch' or community. We add a spatial structure by analysing a set of tritrophic UPCA patch models interconnected by diffusive migration of strength D to form what might constitute a 'metacommunity'[22] (Box 1, equation (2)). We first examine the mutual interaction of two different patches (u_1, v_1, w_1) and (u_2, v_2, w_2) that show UPCA which, in the absence of migration ($D = 0$), would normally be unsynchronized. As the natural frequency Ω_i ($i = 1, 2$) of each uncoupled chaotic community is approximately a linear function of herbivore growth b_i, in our scheme different communities are specified by differences in b_i. Thus,

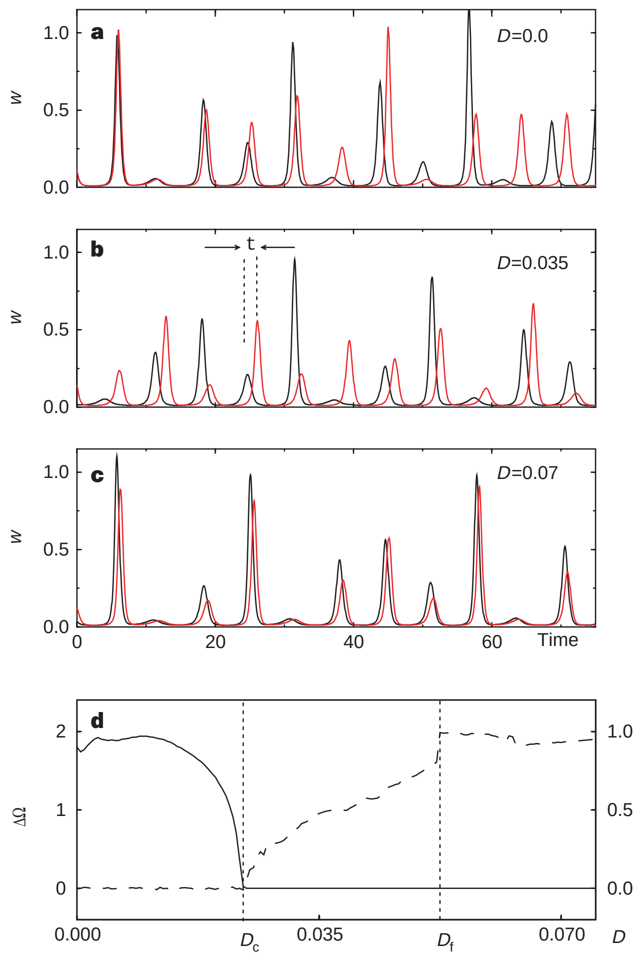

Figure 2 Model time series of predator populations in a two-patch system ($b_1 = 1.1$, $b_2 = 1.055$) under different synchronization regimes. **a**, $D = 0.0 < D_c$ (unsynchronized); **b**, $D = 0.035 > D_c$ (phase synchronized); **c**, $D = 0.07 > D_f$ (full synchronization). **d**, Population time series were decomposed into time-varying phase $\phi(t)$ and amplitude $A(t)$ components (Box 2). For the two-patch system, the relative frequencies, $\Delta\Omega = 100 \times (\Omega_2 - \Omega_1)/\Omega_1$, per cent (solid line), determined using equation (3), together with the correlation r between peak population abundances A_1 and A_2 (dashed line), are plotted as a function of coupling D. Three different regimes are seen: $D < D_c$ (left)–the patches are unsynchronized ($\Delta\Omega > 0$) and slowly drifting in and out of phase, with correlation between peak population abundances $r = 0$; $D_c < D < D_f$ (middle)–the patches are 'phase synchronized' ($\Delta\Omega = 0$), with peak population abundances chaotic but weakly correlated $r \ll 1$; $D < D_f$ (right)–the patches are almost fully synchronized ($\Delta\Omega = 0$), with nearly identical populations and $r \simeq 1$.

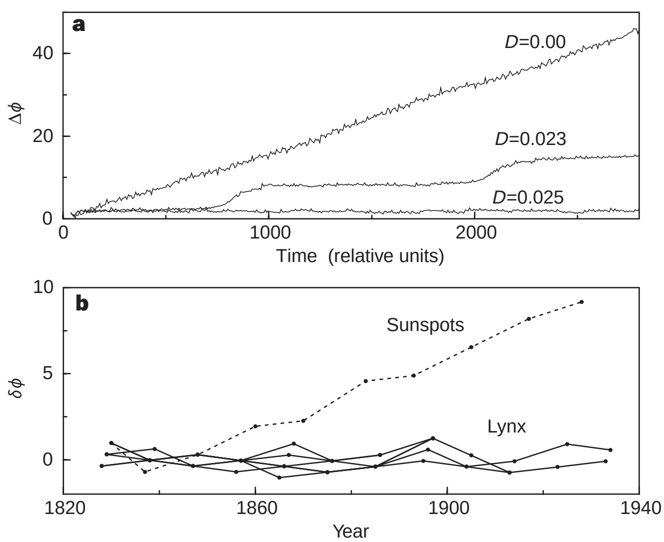

Figure 3 Phase analysis. **a**, Phase growth in two coupled patches. $D = 0$: unsynchronized with linear growth in phase difference between the two patches: $\Delta\phi(t) = \phi_1(t) - \phi_2(t)$, as described by equation (3) (Box 2); $D = 0.025 = D_c$: phase synchronized with constant inter-patch phase difference, $\Delta\phi(t) = \text{const}$; $D = 0.023 \lesssim D_c$: just before the onset of phase synchronization ($D \lesssim D_c = 0.025$), $\Delta\phi$ is generally constant, but sporadically jumps in value as 'phase slips' occur[12]. **b**, Phase growth of the lynx data (from Fig. 1a). For each year, the mean phase growth $\bar{\phi}(t) = \langle\phi_i(t)\rangle$ is calculated as an average over all six regions, $i = 1.6$. For each region, the deviation of the phase growth from the mean ($\delta\phi_i(t) = \bar{\phi}(t) - \phi_i(t)$) is plotted. The phase growth of the filtered sunspot data, $\phi_s(t)$, in the same years (1821–1934) is compared to the mean lynx phase growth, $\bar{\phi}(t)$, by plotting $\delta\phi_s(t) = \bar{\phi}(t) - \phi_s(t)$ (Box 2).

$\Delta\Omega = \Omega_1 - \Omega_2 \simeq b_1 - b_2$ is the frequency difference between two uncoupled unsynchronized communities.

Might these chaotic foodweb systems mutually synchronize after coupling and, if so, how? Although much is known about the synchronization of periodic oscillators, chaotic systems are less well understood[12]. Consider the two-patch UPCA model (Box 1, equation (2)) under conditions of extremely weak coupling. When migration between patches is less than a numerically determined critical value ($D < D_c = 0.025$), the two patches retain their own intrinsic chaotic dynamics, and their populations remain completely independent and unsynchronized, both in amplitude and phase (Fig. 2a). It can be seen and quantitatively shown (Fig. 3a; Box 2) that the two communities cycle at different natural frequencies. In contrast, relatively strong coupling (above a numerically determined threshold; $D > D_f = 0.053$) induces a state of 'complete' or 'full' synchronization[23]. Here, comparable populations in different patches are identical (that is, $u_1(t) = u_2(t)$, $v_1(t) = v_2(t)$, $w_1(t) = w_2(t)$), or very close to identical, even though the dynamics remain chaotic in time (Fig. 2c). Now the two communities entrain one another and cycle chaotically at the same frequency.

A more unusual form of synchronization emerges at weak or intermediate coupling levels ($D_c < D < D_f$). In this case, the predator populations (w_i) in each patch remain synchronized or locked in phase, but their peak population abundances appear to be independent, having very weak correlation (Fig.. 2b). This phase synchronization implies that populations may be synchronized only in phase but not in amplitude[12]. Because of its subtle nature, phase synchronization has been overlooked in population studies before now, but it may be very important because it occurs in the biologically realistic situation of weak coupling. The foodweb model provides one illustration of phase synchronization that closely matches the observed long-term dynamics of lynx populations (Fig. 1a). Although they are synchronized in phase, the populations of each patch nevertheless differ by a theoretically predicted[24] time lag (τ), the implications of which are discussed below. A summary of all synchronization regimes of the foodweb model is given in Fig. 2d.

Various realistic extensions of the foodweb model were analysed to check the robustness of our results. For example, when the system was simulated with hares and lynx migrating at different speeds, phase synchronization was still achieved over wide parameter ranges (see Supplementary Information). Given that stochasticity is ubiquitous in natural ecologies, we examined the response of the model to different types of noise forcing. When the parameters of the model were selected to give a regular periodic cycle and it

Box 2 Analysing phase dynamics in model and natural time series

We devised a practical method to identify subtle forms of synchronization in irregular or chaotic population time series. A cyclic variable $x(t) = A(t)\sin(\phi(t))$ may be decomposed into a time-dependent amplitude $A(t)$ and phase $\phi(t)$, although the decomposition is non-trivial for a chaotic signal[12,13]. We calculate growth in phase ϕ in a time-varying (possibly chaotic) signal $x(t)$ simply by noting that the time between two successive peaks or maxima of $x(t)$ corresponds to an increase of 2π. Hence the instantaneous phase $\phi(t)$ at time t may be determined through linear interpolation after calculating the local rates at which maxima occur in the population time series. The amplitude $A(t)$ of the signal is defined here as the peak population abundance measured stroboscopically as each maximum occurs.

This decomposition technique can be used for detecting phase synchronization in two different population time series, with phases $\phi_1(t)$ and $\phi_2(t)$, respectively. Synchronization may be observed by monitoring the growth in time of the phase difference $\Delta\phi(t) = \phi_1(t) - \phi_2(t)$. When synchronized, $\Delta\phi(t)$ is, on average, constant in time and the two populations lock to the same frequency (frequency difference $\Delta\Omega = 0$). The patches are unsynchronized ($\Delta\Omega > 0$) when the average phase difference $\Delta\phi(t)$ grows with time according to:

$$\Delta\phi(t) = \Delta\Omega \cdot t + \tau \qquad (3)$$

where the time-lag τ acts as a constant offset.

Monitoring phase evolution has many practical applications. For example, it provides an alternative test for checking whether the sunspot cycle entrains the hare–lynx populations[5,25,26]. We analysed the phase growth of the Canadian lynx data over six geographically disparate regions (Fig. 1) and found it to be significantly faster than the phase growth of the sunspot cycle ($P < 0.01$; Fig. 3b). The average period lengths of the lynx and sunspot cycles were determined by regression as $T_l = 9.5 \pm 0.04$ (s.e.) and $T_s = 11.14 \pm 0.015$ (s.e.) years, respectively. Hence, in the long term, sunspot activity is unlikely to be involved in the continual entrainment of the hare–lynx cycle[6,7]. On the other hand, the patterns in phase evolution between the six lynx populations were not significantly different, indicating phase synchronization over all six regions. In addition, the correlations between peak population abundances examined over all pairs of lynx populations were weak, with average $\langle r \rangle = 0.3$, making this synchronization akin to the phase synchronization observed in the model runs above.

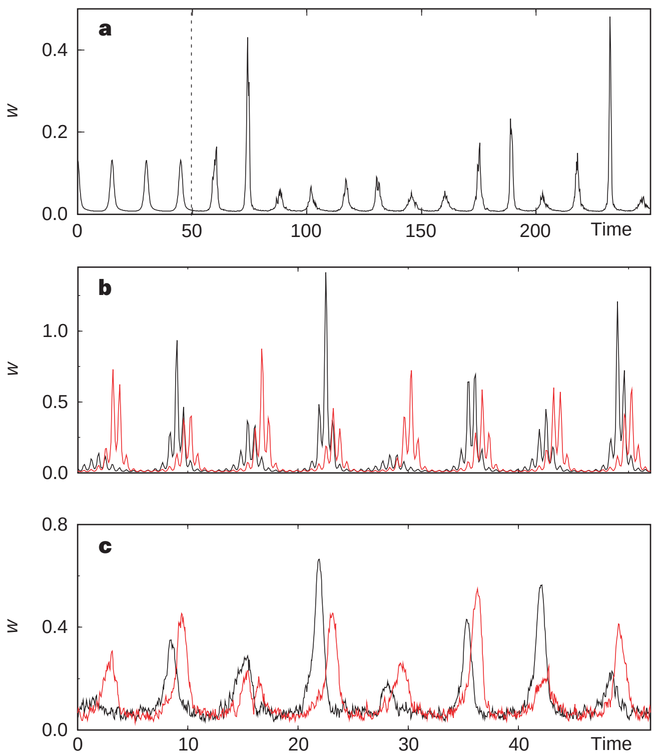

Figure 4 Effects of noise and seasonality. **a**, Noise-induced chaos. When the foodweb model is parametrized according to Box 1, but with $b = 0.2$, a limit-cycle solution results. At $t = 50$, environmental noise was added to the parameters a, b, c in equation (1) with, for example, $a'(t) = a(1 + e(t))$, where $e(t) \simeq N(0, 0.05)$, and so on. The time series exhibited noise-induced chaos with the same UPCA dynamics as the deterministic model (equation (1)) (Fig. 1c). **b**, Robustness of phase synchronization to seasonal forcing. Seasonal forcing was added to the growth rates a, b, c in equation (1) with, for example, $a'(t) = a(1 + 0.1\sin(w_o t))$ for the two patch model parametrized as in Fig. 2b. The frequency, w_o, of the forcing was chosen so that the intrinsic population cycle of the foodweb comprised ten seasonal cycles. The resulting population dynamics realistically portray seasonal dynamics, and the lynx populations (w) of the two-patch system remain in phase synchronization. **c**, Robustness of phase synchronization to noise. Demographic noise was added to all populations in the two-patch chaotic model (by adding noise to the right-hand side of all equations in equation (1)) parametrized as in Fig. 2b. The noise has mean zero and $\sigma = 0.08$ but is restricted so that at any instant the sum of the noise perturbation and the population level remains positive. Despite the noise forcing, the populations remain in phase synchronization.

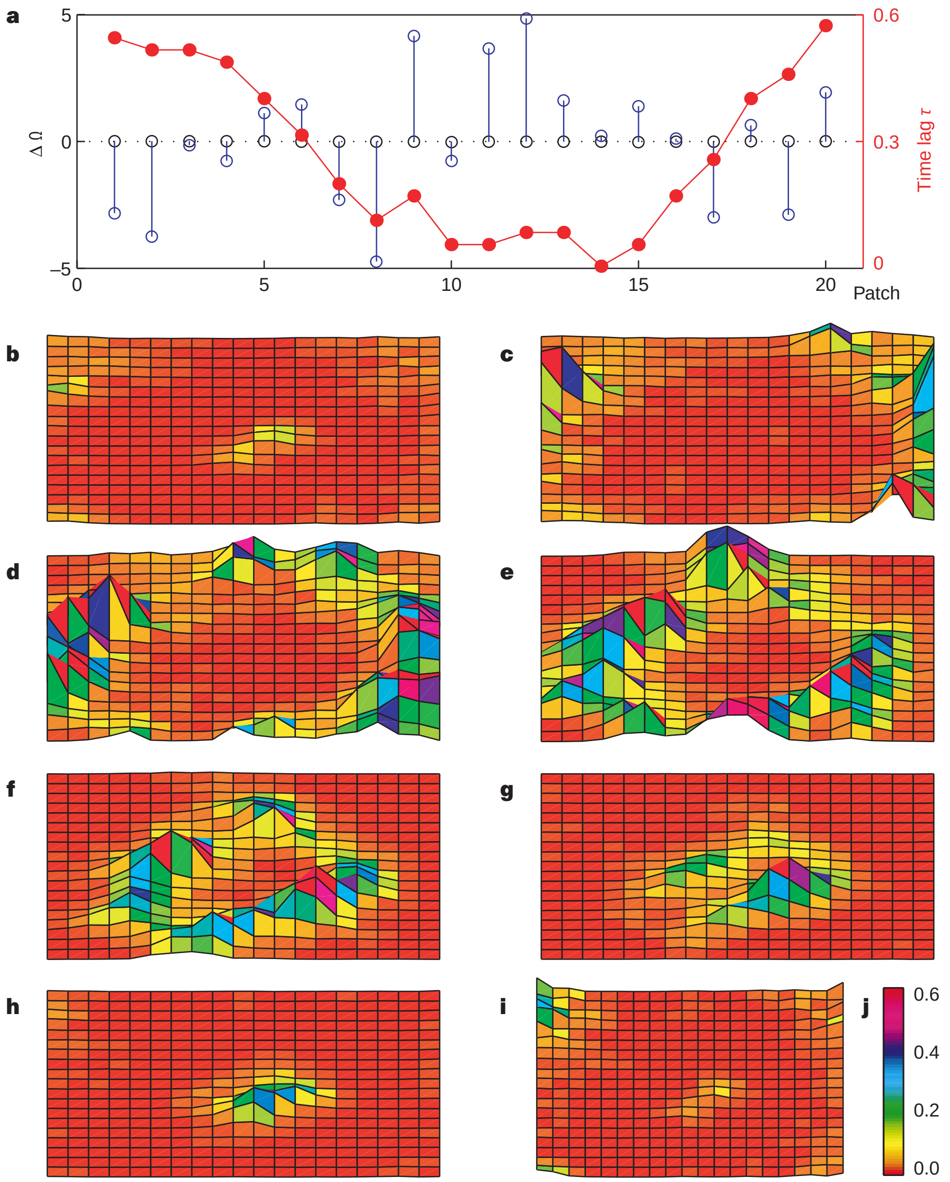

Figure 5 Simulation results in a square lattice of 20 × 20 sites with periodic boundary conditions (Box 1). **a**, For the 20 sites along the lattice diagonal with mean frequency $\bar{\Omega}$, we define the relative frequency of each patch as $\Delta\Omega_i = 100 \times (\Omega_i - \bar{\Omega})/\bar{\Omega}$. The relative frequencies $\Delta\Omega_i$ along the diagonal are plotted for $D = 0$ (blue) and $D = 0.035$ (black). Superimposed is a plot of τ_i (red), the time lag between the maximum of the predator abundance in the ith patch and the maximum of a central reference patch, for the 20 diagonal patches determined when $D = 0.035$ (phase synchronization). Hence τ_i is measured as a fraction of the period length $T = 2\pi/\bar{\Omega}$. The distribution of the τ_i confirms the characteristic 'U' shape found in analyses of the field data[10,25–27]. **b**–**i**, Evolution of a chaotic travelling wave: snapshots of predator abundance in the lattice at 8 consecutive time steps over one period ($D = 0.035$). The wave pattern in **b**–**i** repeats in an endless cycle, with patches having chaotic amplitudes, making each cycle different from the next. **j**, Colour bar shows abundance levels.

was forced with environmental or demographic stochasticity, an unusual form of noise-induced chaos resulted (Fig. 4a). The population dynamics exhibited the same UPCA oscillations as the purely deterministic model (Fig. 1c). In the coupled two-patch foodweb model, neither short-term noisy fluctuations (such as measurement, demographic or environmental noise) nor long-term seasonal changes interfered with the transition to phase synchronization (Fig. 4b, c). In all cases that showed phase synchronization, the actual transition to synchronization was rapid and emerged after only two or three population cycles. Synchronization transitions were found to be complex functions of parameter values (see Supplementary Information).

Finally, we constructed a spatial lattice of $N \times N$ non-identical patch foodwebs (where N was 20, 50 or 100), with each patch consisting of a single tritrophic model (equation (1)) linked by migration to its eight nearest neighbours. All patches were given random consumer growth rates, b_i, uniformly distributed to lie within ±10% of the mean $\langle b_i \rangle = 1$. As expected, with no migration between patches ($D = 0$), the populations displayed independent and unsynchronized chaotic oscillations which varied by ±5% from the mean frequency (Fig. 5a). However, with very low migration ($D = 0.035$), the entire lattice became phase synchronized to a common coherent frequency (Fig. 5a). Despite the strong phase-locking, the 'amplitudes' of patch populations were only weakly correlated ($\langle r \rangle = 0.2$ between all patch pairs).

Note that if all patches were in 'full synchronization', their phase and amplitude dynamics would be identical and populations across the entire lattice would increase and decrease simultaneously. However, when they are phase-synchronized, inter-patch populations peak almost, but not quite, concurrently, with the peaks of pairs of populations being temporally separated by a time lag (as in Fig. 2b). When viewed over a large metacommunity, the time lags show a characteristic 'U' shape (Fig. 5a). This gives rise to a remarkable chaotic travelling-wave structure which may be seen in the eight lattice 'snapshots' of Fig. 5b–i. Population abundances in the meta-community remain chaotic, but periodic circular waves continuously expand and contract radially as they spread in time across the spatial landscape. Field and model population studies of the Canadian hare–lynx cycle and European vole cycles have found similar travelling-wave structures with spatially distributed U-shaped phase lags[10,25–27]. Different types of realistic diffusion barrier were introduced into the model but, in general, they failed to destroy the spatial circular wave structure (B.B. *et al.*, manuscript in preparation).

The spatio-temporal structures associated with phase synchronization have important implications for conservation ecology. Even if a disturbance perturbs a local patch population to the brink of extinction, the periodicity of spatial phase syncrhonization guarantees the recurring arrival of wave fronts in which new colonizers will buffer the endangered population. In contrast to the common view of population synchronization as a cause of global population extinctions[14], it appears that phase synchronization can be important for maintaining species persistence. Our findings indicate that synchronization is a powerful process that has the potential to shape the distribution and abundance of species over all scales, from local to continental. We expect that the complex synchronization phenomena identified here will provide new insight into the dynamics of spatial ecologies and will have important applications to the study of biological rhythms in general. □

Received 22 January; accepted 29 March 1999.

1. Elton, C. & Nicholson, M. The ten-year cycle in numbers of the lynx in Canada. *J. Anim. Ecol.* **11,** 215–244 (1942).
2. May, R. M. *Stability and Complexity in Model Ecosystems* (Princeton University Press, Princeton, 1973).
3. Keith, L. B. *Wildlife's 10-year cycle* (University of Wisconsin Press, Madison, 1963).
4. Hanski, I., Turchin, P., Korpimaki, E. & Henttonen, H. Population oscillations of boreal rodents: regulation by mustelid predators leads to chaos. *Nature* **364,** 232–235 (1993).
5. Sinclair, A. R. E. *et al*. Can the solar cycle and climate synchronize the snowshoe hare cycle in Canada? Evidence from tree rings and ice cores. *Am. Nat.* **141,** 173–198 (1993).
6. Royama, T. *Analytical Population Dynamics* (Chapman & Hall, London, 1992).
7. Moran, P. A. P. The statistical analysis of the Canadian lynx cycle. *Aust. J. Zool.* **1,** 291–298 (1953).
8. Bulmer, M. G. A statistical analysis of the 10-year cycle in Canada. *J. Anim. Ecol.* **43,** 701–718 (1974).
9. Korpimaki, E. & Krebs, C. J. Predation and population cycles of small mammals. A reassessment of the predation hypothesis. *BioScience* **46,** 754–764 (1996).
10. Ranta, E., Kaitala, V. & Lundberg, P. The spatial dimension in population fluctuations. *Science* **278,** 1621–1623 (1997).
11. Schaffer, W. Stretching and folding in lynx fur returns: Evidence for a strange attractor in nature? *Am. Nat.* **124,** 798–820 (1984).
12. Rosenblum, M. G., Pikovsky, A. S. & Kurths, J. Phase synchronization of chaotic oscillators. *Phys. Rev. Lett.* **76,** 1804–1807 (1996).
13. Schafer, C., Rosenblum, M. G., Kurths, J. & Abel, H. Heartbeat synchronized with ventilation. *Nature* **392,** 239–240 (1998).
14. Earn, D. J. D., Rohani, P. & Grenfell, B. Persistence, chaos and synchrony in ecology and epidemiology. *Proc. R. Soc. Lond. B* **265,** 7–10 (1998).
15. May, R. M. Simple mathematical models with very complicated dynamics. *Nature* **261,** 459–467 (1976).
16. Stone, L. Period-doubling reversals and chaos in simple ecological models. *Nature* **365,** 617–620 (1993).
17. Blasius, B., Neff, R., Beck, F. & Lüttge, U. Oscillatory model of Crassulacean acid metabolism with a dynamic hysteresis switch. *Proc. R. Soc. Lond. B* **266,** 93–101 (1999).
18. Gurney, W. S. C., Crowley, P. H. & Nisbet, R. M. Locking life-cycles on to seasons: circle-map models of population dynamics and local adaptation. *J. Math. Biol.* **30,** 251–279 (1992).
19. Hastings, A. & Powell, T. Chaos in a three-species food chain. *Ecology* **72,** 896–903 (1991).
20. Gilpin, M. E. Spiral chaos in a predator–prey model. *Am. Nat.* **107,** 306–308 (1979).
21. Vandermeer, J. Seasonal isochronic forcing of Lotka Volterra equations. *Progr. Theor. Phys.* **71,** 13–28 (1996).
22. Gotelli, N. J. *A Primer of Ecology* (Sinauer, Massachusetts, 1995).
23. Pecora, L. M. & Carroll, T. L. Synchronization in chaotic systems. *Phys. Rev. Lett.* **64,** 821 (1990).
24. Cohen, A. H., Holmes, P. J. & Rand, R. H. The nature of the coupling between segmental oscillators of the lamprey spinal generator for locomotion: a mathematical model. *J. Math. Biol.* **13,** 345–369 (1982).
25. Ranta, E. *et al*. Solar activity and hare dynamics: A cross-continental comparison. *Am. Nat.* **149,** 765–775 (1997).
26. Sinclair, A. R. E. & Gosline, M. Solar activity and mammal cycles in the northern hemisphere. *Am. Nat.* **149,** 776–784 (1997).
27. Ranta, E. & Kaitala, V. Travelling waves in vole population dynamics. *Nature* **390,** 456 (1997).
28. Stenseth, N. C., Falck, W., Bjornstad, O. N. & Krebs, C. J. Population regulation in snowshoe hare and Canadian lynx: Asymmetric food web configurations between hare and lynx. *Proc. Natl Acad. Sci. USA* **94,** 5147–5152 (1997).
29. O'Donoghue, M. *et al*. Functional response of coyotes and lynx to the snowshoe hare cycle. *Ecology* **79,** 1193–1208 (1998).
30. Wolf, J. B., Swift, H. L. & Vastano, J. A. Determining Lyapunov exponents from a time series. *Physica D* **16,** 285–317 (1982).

Supplementary information is available on *Nature*'s World-Wide Web site (http://www.nature.com) or as paper copy from the London editorial office of *Nature*.

Acknowledgements. We thank MINERVA for their award of a Fellowship to B.B., and H. Bhasin for her comments on the manuscript.

Correspondence and requests for materials should be addressed to L.S. (e-mail: lewi@lanina.tau.ac.il).

Auditory collusion and a coupled couple of outer hair cells

Hong-Bo Zhao & J. Santos-Sacchi

Sections of Otolaryngology and Neurobiology, Yale University School of Medicine, 333 Cedar Street, New Haven, Connecticut 06510, USA

The discrepancies between measured frequency responses of the basilar membrane in the inner ear and the frequency tuning found in psychophysical experiments led to Békésy's idea of lateral inhibition in the auditory nervous system[1]. We now know that basilar membrane tuning can account for neural tuning[2], and that sharpening of the passive travelling wave depends on the mechanical activity of outer hair cells (OHCs)[3], but the mechanism by which OHCs enhance tuning remains unclear. OHCs generate voltage-dependent length changes at acoustic rates[4–8], which deform the cochlear partition[9–11]. Here we use an electrical correlate of OHC mechanical activity, the motility-related gating current, to investigate mechano-electrical interactions among adjacent OHCs. We show that the motility caused by voltage stimulation of one cell in a group evokes gating currents in adjacent OHCs. The resulting polarization in adjacent cells is opposite to that within the stimulated cell, which may be indicative of lateral inhibition. Also such interactions promote distortion and suppression in the electrical and, consequently, the mechanical activity of OHCs. Lateral interactions may provide a basis for enhanced frequency selectivity in the basilar membrane of mammals.

The mechanical response of the OHC is mirrored by an electrical signature, a motility-related charge movement, similar to the gating charge movements that control ion-channel conductance[12,13]. Both gating currents arise from a redistribution of charged voltage sensors across the membrane. The magnitude of the gating current reflects the rate of charge redistribution. In the OHC, the redistribution of motility-related charge is controlled by both voltage and membrane tension; consequently, either can evoke gating currents[14–16]. Within the organ of Corti, OHCs are indirectly mechanically coupled to each other through contacts with supporting Deiters' cells. The apical regions of OHCs and Deiters' cells are joined by tight junctions and form the plate-like reticular lamina. Basally, the OHCs sit in the cups of Deiters' cells, and the strength of these attachments varies along the length of the basilar membrane[17]. This morphology makes it likely that the voltage-induced mechanical responses of one OHC will affect surrounding OHCs. Determining the nature of this interaction may provide insight into the process of fine frequency tuning by OHCs. We studied this interaction by simultaneously recording from adjacent OHCs under dual whole-cell voltage and current clamp.

In isolated pieces of Corti's organ, where cellular relations remain intact, voltage stimulation of an OHC induces mechanical responses and gating currents in that cell (Fig. 1). Transient outward currents are generated by the onset of depolarization, which causes the cell to contract (Fig. 1b). These currents correspond to the displacement of positive charge to the extracellular aspect of the lateral plasma membrane, which holds motility/voltage sensors[18,19]. The charge–voltage (Q–V) function is well described by a two-state